ELSEVIER

Biophysical Chemistry 104 (2003) 605–616

Biophysical Chemistry

www.elsevier.com/locate/bpc

Comparison of two different lysozyme types under native and crystallization conditions using two-dimensional NMR and dynamic light scattering

Jaroslaw Poznański[a,b,*], Yannis Georgalis[c], Lorin Wehr[d], Wolfram Saenger[d], Piotr Zielenkiewicz[a,e]

[a]*Institute of Biochemistry and Biophysics, Polish Academy of Sciences, Pawińskiego 5A, 02-106 Warsaw, Poland*
[b]*Institute of Physical Chemistry, Polish Academy of Sciences, Kasprzaka 44/52, 01-224 Warsaw, Poland*
[c]*Triton-Hellas, Plateia Demokratias, 1 Egnatia Buildings, 54629 Thessaloniki, Greece*
[d]*Institute of Crystallography Freie Universität Berlin, Takustrasse 6, 14194 Berlin, Germany*
[e]*Institute of Experimental Plant Biology, Warsaw University, Miecznikowa 1, 02-096 Warsaw, Poland*

Received 20 December 2002; received in revised form 10 March 2003; accepted 11 March 2003

Abstract

In order to elucidate differences observed in the aggregation kinetics of hen-egg white lysozyme under crystallization conditions we have undertaken a comparative study of the enzyme marketed by Seikagaku and Sigma companies. When the crystallization of the two lysozyme preparations is followed by time-resolved dynamic light scattering, the structural differences are also observed under native conditions in the early nucleation kinetics. The differences are manifested in the formation rates of macroscopic crystals, but do not influence the morphology of the typical tetragonal lysozyme crystal. Using two-dimensional NMR we have followed the differences in the native-like solution structure of the two preparations, while the primary sequence and molecular mass are identical. According to the published structure of tetragonal lysozyme crystal the largest deviations were found for the residues involved in the intermolecular interactions in crystal structure.

Keywords: Lysozyme; NMR; Dynamic light scattering; Early nucleation

1. Introduction

Hen-egg white lysozyme has been exhaustively used the past decade as a model for elucidating the mechanism of protein crystal growth. Despite the conflicts found in literature, recent consensus indicates that protein crystallization is not much different from that of inorganic compounds (for a review see [1]). Among first-order phase transitions, crystallization and melting processes in atomic solids have a long and respectable research history. In protein nucleation, however, the kinetics of the phase transition is not yet understood in depth. Muschol and Rosenberger [2,3] attributed the behaviour of supersaturated lysozyme solutions to non-ideality. The same group also presented the effect of impurities and micro-heterogeneities in

*Corresponding author. Tel.: +48-22-658-47-24; fax: +48-39-12-16-23.
E-mail address: jarek@ibb.waw.pl (J. Poznański).

0301-4622/03/$ - see front matter © 2003 Elsevier Science B.V. All rights reserved.
doi:10.1016/S0301-4622(03)00061-9

lysozyme solutions. There is no doubt that several issues still have to be clarified but much of these discrepancies can be attributed to the applied procedures (i.e. centrifuged vs. non-centrifuged solutions upon addition of electrolyte, data evaluation approaches etc.). If one attributes these properties of supersaturated protein solutions to non-ideality it is, however, unclear how nuclei could grow out of stationary solutions. Much earlier than we did experimentally, the same group has theoretically shown that fractals resemble a probable morphological instability step during crystal growth [4,5]. Tanaka et al. verified the coexistence of oligomers and clusters in supersaturated lysozyme solutions [6] using time-resolved dynamic light scattering (DLS), corroborating our findings. Their analyses indicated growth exponents of approximately -0.50, in fair agreement to the reciprocal fractal dimension for DLCA-like aggregation, 0.55, and power-law kinetics, exactly as in our case. The authors claimed globular clusters with a conserved order parameter invoking Langer's work [7]. Whether this interpretation is correct depends on many factors, and conclusions cannot be drawn yet with confidence. The observed differences can be attributed to variations of the initial experimental conditions such as temperature, pH, polydispersity and origin of lysozyme. As already mentioned, it is possible to observe wide variations on growth exponents by varying only slightly the initial conditions. The approximate number of larger clusters was also found in fair agreement with that determined by us. This is the first report that unequivocally demonstrates the formation of large clusters in nucleating lysozyme solutions and renders support to our works. In a subsequent work [8] several morphological instabilities were shown during nucleation of lysozyme, similar to our observations. These instabilities were interpreted as a competition process between liquid–liquid and liquid–solid phase separation. In our previous works we have examined most often commercial hen-egg white lysozyme preparations, purchased from Sigma Chemical Co. Using time-resolved DLS [9,10] we have found out, nearly without any exception, that Sigma preparations exhibit small differences, even when precautions for assuring reproducible growth kinetics are taken. However, even more pronounced were differences in lysozymes purchased from different companies. Depending on additional treatment (dialysis, chromatographic purification, lyophilization, etc.) one may amplify or diminish such differences. In this work we address the question of how critical is the starting material. We have compared two hen-egg white lysozyme preparations purchased from Seikagaku and Sigma, purposely used without further purification. To interpret differences often observed in macroscopic crystal growth rates one usually speculates on unknown impurities, variability in the folded lysozyme population, strongly bound ions etc. Most times there is no way to really persuasively prove these ideas. The worst impurity seems to us to be the precipitating agent and randomly permutated cocktails used to force proteins to crystallize. In this work we have combined NMR, and time-resolved DLS to compare two lysozyme types. Structural differences indicated by the NMR spectra in native lysozyme types are also detected by DLS upon ignition of the crystallization reaction by a suitable electrolyte (NaCl). The system lysozyme-NaCl is simple and nucleation kinetics can be monitored with confidence using DLS.

2. Results

2.1. Samples homogeneity test

Both lysozyme probes analysed by the mass spectrometry demonstrate almost identical m/z pattern indicating the molecular mass of 14300D (Fig. 1). The identity of the envelope curves obtained for both m/z patterns clearly indicate almost the same charge carriage propensity of both samples, including any cation binding. Deconvoluted mass spectra directly proved absence of any highly populated cationic adducts, the only differences could be attributed to the existence in the Sigma stock a small amount of the compound of 14460.4D, which is probably glycosylated protein (cf. insets in Fig. 1).

Detailed analysis of the 2D-TOCSY spectra of both stocks proves no evident sequential differences (Fig. 2). Additional TOCSY spectrum of the

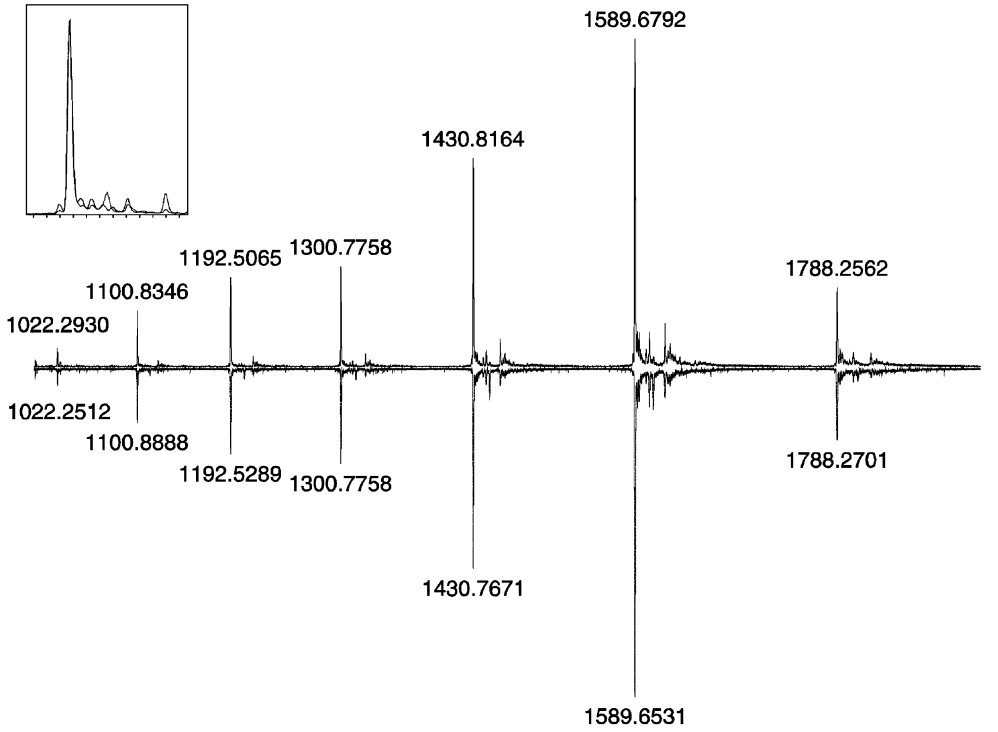

Fig. 1. TOF MS ES+mass spectra of Sigma (upper, solid trace) and Seikagaku (mirrored, dotted trace) lysozyme probes. Both preparations exhibit almost identical major m/z peak pattern corresponding to the molecular mass of 14300D. Similar m/z envelope curves indicate identical distribution of the molecular ions in electrospray analysis. The estimated mass distribution (inset) indicate the low population of any cations bounded to the protein samples. The deviations in minor m/z peak patterns are mainly arising from low populated lysozyme adducts of the mass 160.4D.

1:1 mixture of both lysozyme samples (not presented) showed the single set of the cross-peaks in the fingerprint region of the spectrum, clearly indicating no sequential differences between both stocks.

2.2. Chemical shift analysis

For both lysozyme samples almost all proton resonances were assigned. Comparison of the obtained chemical shift values to the published data of Sigma lysozyme [11] was made separately for both samples. Fig. 3a and b demonstrate that Seikagaku lysozyme deviates from the 1988-year Sigma sample much more than the presently used Sigma lysozyme sample does. The root mean square deviation of the chemical shift calculated for amide protons equals 8.6 Hz for Seikagaku lysozyme and 5.3 Hz for Sigma lysozyme as well as 5.2 and 4.0 Hz for Hα protons, respectively, (neglecting different assignment of Trp111 Hα). The largest differences (exceeding 10 Hz) between Seikagaku lysozyme and Sigma lysozyme are observed for amide protons of Met12, Arg14, Asn19, Asn44, Gln57, Asn59, Trp62, Cys80, Val99, Asp101, Asn103 Ala107 and Hα protons of Gly22, Cys30, Thr69, Cys80, Ala95, Ser100, Asp101, Gly102, respectively. In most cases the chemical shift deviations in Fig. 4A could not be attributed to a direct effect of electrostatic screening of the close acidic residues.

The used method of the manual pH adjustment of the NMR probes resulted in small pH differences (<0.1), which might drive the protonation equilibrium of the acidic residues (according to the pK's Asp$\approx$3.6; Glu$\approx$4.3) e.g. Glu7, Asp18,

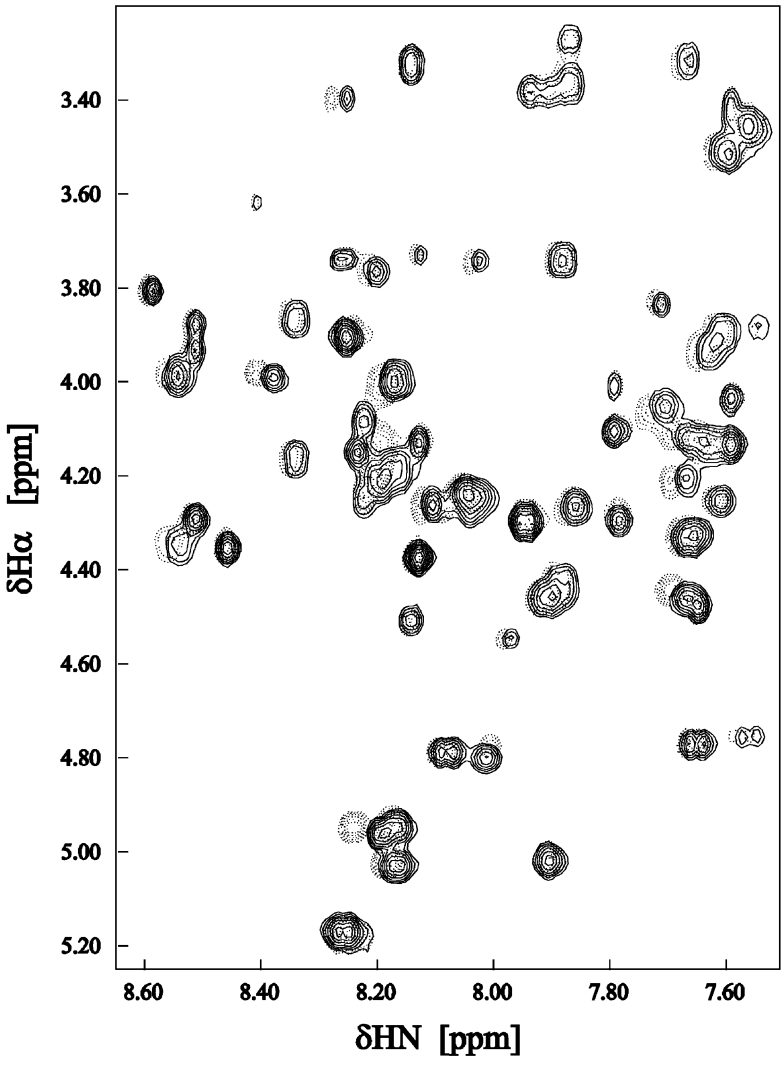

Fig. 2. Fingerprint regions of the TOCSY spectra obtained for Seikagaku (dotted line) and Sigma (solid line) lysozyme probes. The differences in resonance localizations arise from small deviations in the lysozyme conformation and/or intermolecular interactions pattern.

Glu35, Asp48, Asp52, Asp66, Asp87, Asp101 and Asp119. The latter was monitored by the analysis of the chemical shift of the terminal methylene groups adjacent to the carboxylate group e.g. Asp $C\beta H_2$ and Glu $C\gamma H_2$. Data presented in the Table 1 prove that the only significant difference in the putative protonation equilibrium could be attributed to Asp52 and Asp101 residues, which are found in quite different locations. Proton chemical shifts of Asp101, located between the end of the Thr89–Ser100 helix and the Asn103–Asn106 type II′ β-turn, are distorted analogously to the chemical shifts of close in the sequence residues (Val99, Asp101, Gly102, Asn103), whereas Asp52 located in the Ser50–Tyr53 beta sheet influences mostly the partners in the opposite chain of the β-strand.

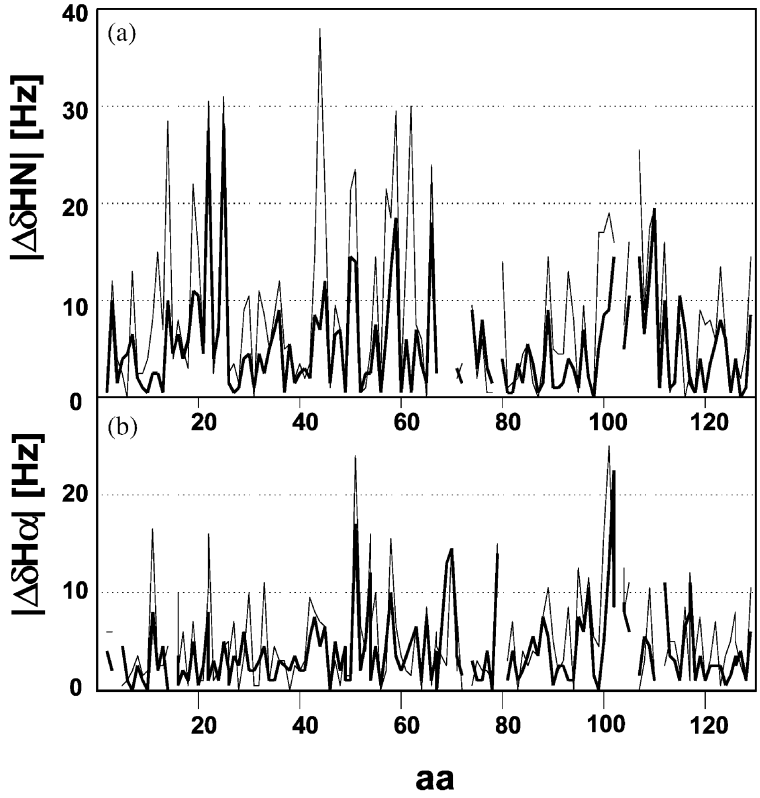

Fig. 3. Sequential distribution of the absolute value of the chemical shift deviation of Seikagaku lysozyme (thin line) and Sigma lysozyme (thick line) from published data of Sigma lysozyme stock [11] calculated for amide (a) and Hα (b) protons.

The relatively large chemical shift differences observed for all Asp101 protons strongly suggest that despite the possible change of the Asp101 protonation equilibrium, lysozyme probes differ significantly in the Asp101 spatial neighbourhood involving a hydration and/or a conformational change. The effect of chemical shift change observed for only $C\beta H_2$ Asp52 methylene protons could be directly assigned to the pH induced difference of the carboxyl group protonation equilibrium.

2.3. Time-resolved DLS experiments

Using DLS the monomeric lysozyme radius, under native conditions, was found to be slightly below 2 nm. This value corresponds to a diffusion coefficient of $(10.86 \pm 0.07) \times 10^{-7}$ cm^2 s^{-1} corrected for water and 293.2 K for both lysozyme types, which also exhibited low polydispersity ($<10\%$).

The final output of the experiments conducted with Seikagaku and Sigma lysozyme are shown in Fig. 6a–c and d–f, respectively. In aggregation experiments we usually observe two predominant populations. One corresponds to monomeric or oligomeric species whose mean apparent hydrodynamic radii, R_h, are stationary, and their relative amount is reduced with time since they are consumed to form larger clusters. The radii of the stationary species shown in Fig. 6 appear to be larger than that of the monomer due to attractive interactions among monomers induced upon addition of NaCl. When the hydrodynamic radii (or

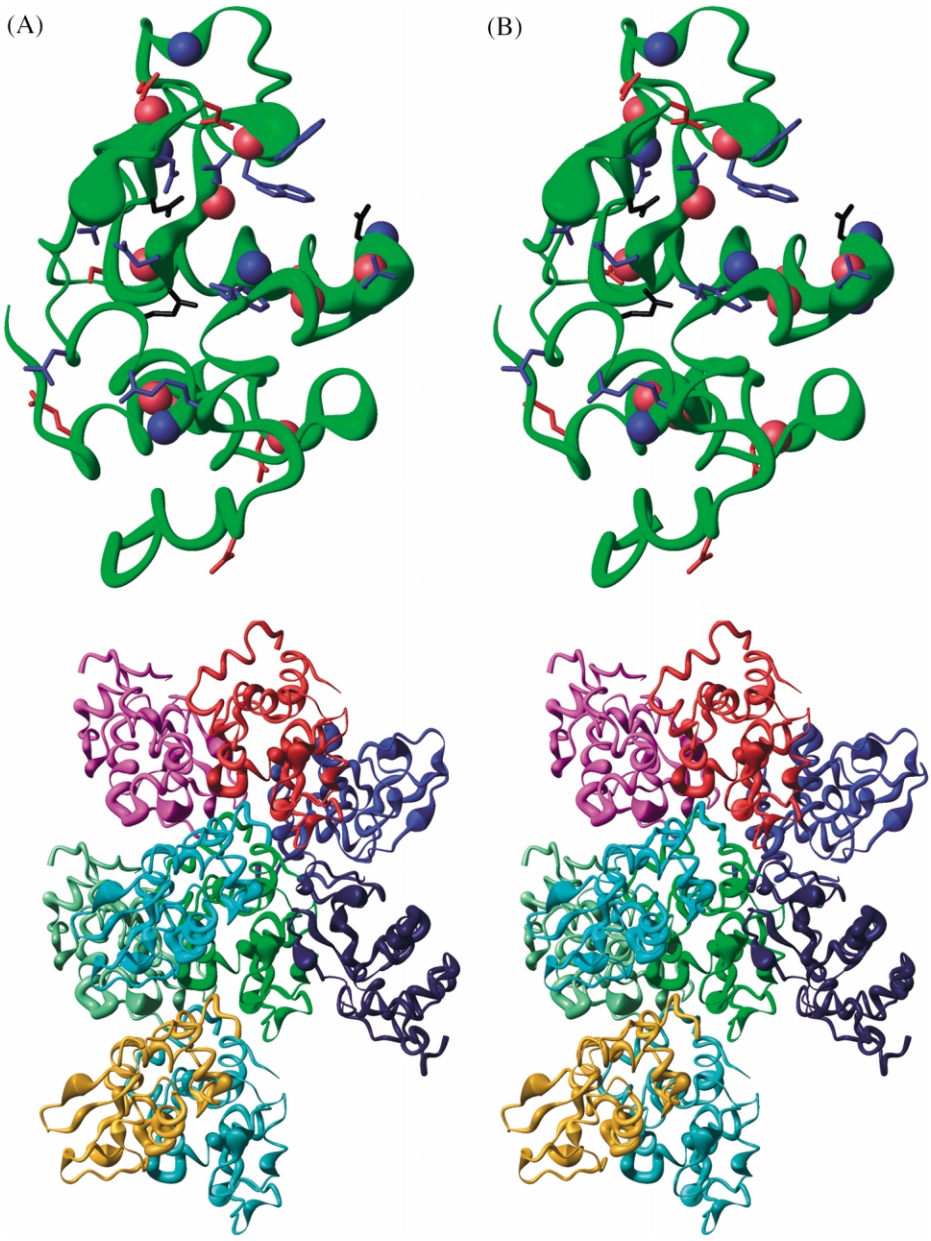

Fig. 4. (A) Schematic representation of the amide proton chemical shift difference between Seikagaku lysozyme and Sigma lysozyme. The side-chains of acidic residues marked in red, residues involved in enzymatic activity are marked in blue and Asp52, Glu35, Asp101 in black. Protons exercising $\Delta\delta > 10$ Hz marked by green (Hα) and blue (HN) balls, respectively. (B) Stereo representation of the intermolecular contacts in tetragonal lysozyme crystal. The molecules are coloured individually, the central one in green. For both representations the radius of the tube following the Cα backbone is proportional to the $((\Delta\delta\mathrm{HN})^2+(\Delta\delta\mathrm{H}\alpha)^2)^{1/2}$.

Table 1
Chemical shift differences of the acidic amino acids for the two lysozyme probes

Residue	Chemical shift difference (Hz)					
	HN	Hα	Hβ		Hγ	
Glu7	−6.5	−2.0	−5.0	−11.0	−3.5	−3.5
Asp18	−3.0	1.5	0.0	−6.0		
Glu35	1.5	−3.5	−12.0	3.0	0.0	−0.5
Asp48	0.0	−1.5	−1.0	−1.0		
Asp52	−1.0	−4.5	−18.5	−7.0		
Asp66	6.0	−0.5	2.0	−5.5		
Asp87	−0.5	0.0	0.5	3.5		
Asp101	−10.0	−12.5	−35.5	−35.5		
Asp119	−5.0	−4.0	−5.0	−8.0		

Large deviations for the terminal methylene protons (Asp Hβ and Glu Hγ) indicate the possible difference in the protonation state. Spatial localization of the acidic residues in lysozyme is presented in Fig. 4.

the corresponding diffusion coefficients) typifying this population are plotted as a function of protein concentration (or volume fraction) one retrieves exactly the monomer radius of 2 nm (data not shown). The positive slope of such plots (negative if we plot diffusion coefficients vs. volume fraction) indicates the appearance of substantial attractive forces, responsible for inducing aggregation [12–14].

The other population resembles nucleating species undergoing growth and both preparations exhibit the expected sigmoidal behaviour. Both size and amount of the growing cluster increases with time due to stochastic collisions between nuclei. The outcome of such collisions is large fractal clusters. By using a small scattering volume (100 nl) we were able to clearly decouple the sigmoidal initial nucleation stage (Fig. 5, open circles). The treatment of this process is beyond the scope of the present work. The most important reasons for temporarily neglecting it are experimental ambiguities (i.e. acquisition times are still too long for capturing events unambiguously) and the lack of a sound theoretical basis (the application of homogeneous nucleation from the melt is not directly applicable to heterogeneous protein nucleation).

Seikagaku lysozyme indicates faster initial nucleation kinetics, and clusters with radii ranging between 40 and 100 nm formed immediately upon initiating the reaction. In contrast, the Sigma lysozyme kinetics was slower, the clusters grown at equivalent times had radii approximately 20 nm and the lag phase was more pronounced. Worth noting are the different slopes typifying the linear parts of the kinetics. Sigma lysozyme kinetics indicated formation of tenuous fractal clusters upon completion of the nucleation period. The fractal dimension of these clusters is in the range of 1.60–1.70 indicating a diffusion limited-like cluster–cluster aggregation, in accordance to previous findings [15–18]. In pure diffusion limited cluster–cluster growth the theoretically expected dimension is 1.81 for assuming formation of self-

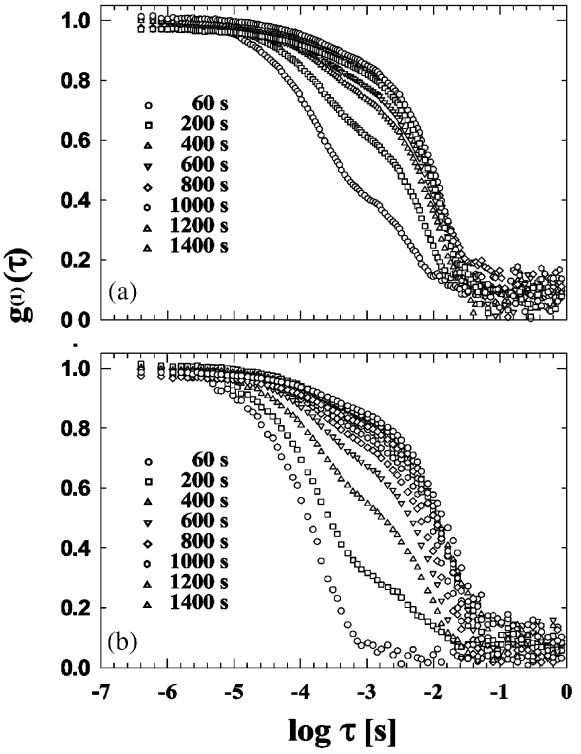

Fig. 5. Comparison of ACF's of (a) Seikagaku and (b) Sigma lysozyme in Na-acetate buffer, pH 4.25. The final lysozyme concentration was 3.5 mM in 0.75 M NaCl. Only every second point of each fifth ACF is plotted for the sake of clarity. Although the spectra should be similar, they exhibit significant differences. Acquisition times are indicated by different symbols.

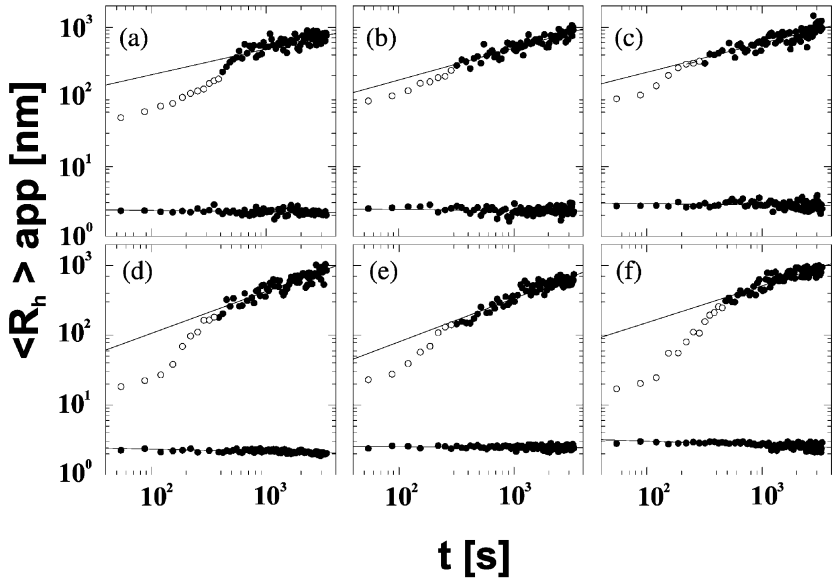

Fig. 6. Time-resolved DLS experiments with 0.7 (a), 2.1 (b) and 3.5 mM (c) of Seikagaku lysozyme incubated with 0.75 M NaCl at pH 4.25. (d), (e) and (f) are their identical counterparts using Sigma lysozyme. The displayed kinetics correspond to averages of two experiments each using the same initial lysozyme concentration. Note the differences typifying both the initial (open circles) and later stages (closed circles) of the aggregation process. Monomer radii (closed triangles) are given in Table 2 and the respective fractal exponents in Table 3.

similar fractals [19]. In contrast, Seikagaku lysozyme clusters indicate a gradual formation of more compact structures at later reaction stages with fractal dimensions ranging between 2.20 and 2.70. We attribute the differences in the late stage exponents to structural changes and/or hydration as indicated in the native enzyme form by two-dimensional NMR. Such changes favour minor differences in screening of lysozyme surface charge which in turn give rise to different dimensionalities throughout.

Visual observations indicated that both lysozyme preparations crystallize successfully under the conditions employed. The crystal habit resembled in both cases the well-known tetragonal form. However, the crystals obtained from Seikagaku lysozyme grew faster than those from Sigma, the observed differences in growth are insignificant,

Table 2
Monomer radius of lysozyme determined at three different concentrations

Lysozyme (mM)	R_h (nm) Seikagaku	R_h (nm) Sigma
0.7	2.21±0.19	2.12±0.11
2.1	2.34±0.25	2.46±0.14
3.5	2.81±0.49	2.62±0.25

The values denote the mean and standard deviation obtained by averaging over all times the duplicate experiments (stationary components only) in 0.75 M NaCl, pH 4.25 shown in Fig. 6.

Table 3
Fractal exponents derived from the experiments shown in Fig. 6

Lysozyme (mM)	d_f Seikagaku	d_f Sigma
0.7	2.70 (0.815)	1.58 (0.803)
2.1	2.20 (0.895)	1.61 (0.859)
3.5	2.34 (0.861)	1.67 (0.801)

The numbers in parentheses denote the squared correlation coefficient of fit into the linear part of each curve. Note the differences in the fractals exponent d_f, which is attributed to differences in the commercial preparation of the enzyme.

i.e. Sigma lysozyme crystals of the same size were visualized 1–2 days later.

3. Discussion

As shown in Fig. 4A, most of the observed significant chemical shift deviations do not result from electrostatic interactions with any acidic residues, whose protonation equilibrium may slightly differ in both probes. Presented data indicates that conformation/neighbourhood of Asp101 changes between probes whereas Asp52 chemical shift deviations may result from change of its protonation equilibrium. According to the NMR chemical shift data the largest differences between the two studied lysozyme probes were found in the surface exposed protein regions, two segments close to helix C-termini (Met12, Arg14, His15 and Val99, Asp101, Gly102, Asn103) as well as four aminoacids close to β-turns (Asn44, Trp62, Thr69, Cys80), respectively. Some of the mentioned residues (Asn44, Asp52, Trp62, Asp101, Asn103) are involved in substrate binding (Phe34 Glu35 Asn37 Asn44 Asn46 Asp52 Gln57 Asn59 Trp62 Trp63 Asp101 Asn103 Ala107 Trp108 Val109 Arg114), which is easily visible in Fig. 4A.

Detailed analysis of the intermolecular interactions occurring in the tetragonal crystal structure of lysozyme demonstrate that the aminoacids exercising relatively large chemical shift differences are located in regions of intermolecular contacts, as it is presented in Fig. 4. Thus Met12–His15 segment is interacting with Glu7, Ala10, Arg128 of the neighbouring molecule I and Val99–Asn103 is close to Arg112, Asn113 of molecule G. Asn44 is interacting with Arg45, and Arg48 of molecule H, Trp62 with Gln121 of molecule E, Cys80 with Gln41 of molecule H. No intermolecular interactions were found for Thr69 and Ala95. It is worth to point out that both HN and Hα proton chemical shifts are conformation sensitive, so weak intermolecular interactions are detectable mainly by structural deformation of less rigid regions, including flexible loops. It may be concluded that the precrystallization states of the lysozyme probes analysed by NMR are tending to reproduce the native intermolecular interactions characteristic for the tetragonal crystal structure. This suggests that both probes of lysozyme differ in the NMR experiment in their patterns of intermolecular interactions, which gave rise to the observed deviations in chemical shifts of the involved aminoacids.

Presented hypothesis is consistent with the analysis of the folded lysozyme flexibility. According to the main chain amide group NMR relaxation experiments [20] Met12–His15, Ans64, Thr69 and Val99–Asn103 residues are located in the relatively disordered ($S^2 < 0.85$) regions. Theoretical calculations [21] demonstrated that Cys30, Cys80 and Ala95 were kinetically hot residues exhibiting large amplitude of high frequency mode of motion.

Thus, the obtained results indicate that the observed changes in chemical shifts undergoes in the surface exposed regions of increased amplitude if internal motion. In consequence small differences in intermolecular contacts result in the detectable changes of experimentally determined chemical proton shifts of described residues.

It is understandable that the growth kinetics, observed by DLS, are modulated by relatively small differences in concentration of any particles (ions, small molecules), in which low populations are not detectable neither by NMR nor by mass spectroscopy. This interactions may reflect the intimate propagation of structural and/or hydration changes of the native enzyme type(s). If such differences are clearly observable with lysozyme, which is a relatively inexpensive and well characterized model system, we believe that more caution than so far anticipated should be exercised when undertaking comparisons in nucleation kinetics.

4. Material and methods

Lysozyme was purchased from Seikagaku (Lot Nr. E94Z06) and from Sigma (Lot Nr. 57H7045). DLS experiments were conducted in Na-acetate buffer pH 4.25. NaCl was purchased from Merck in suprapure form and all other stock solutions were made in fresh, triply distilled water.

Mass spectra were determined on an electrospray (ESI–MS) quadrupole time of flight (Q-Tof) Micromass spectrometer, UK, with resolution approximately 10 000. Spectrometer was calibrated on a bovine pancreatic trypsin inhibitor probe.

NMR experiments were performed on 7 mM samples in a mixture of 90% H_2O–10% ^2H_2O at 308 K. In order to minimize distortions arising from addition of extraneous ions to the probe the pH was carefully adjusted at 3.8 by adding small amounts of 0.2 M HCl. All spectra were recorded on a Varian Unity Plus spectrometer operating at 500 MHz. States [22] method of the quadrature detection of indirect axes was used. Spectra were accumulated with a spectral width of 7200 Hz and 1.3 s relaxation delay. The water signal was suppressed by the use of the WATERGATE [23] pulse sequence where a selective inversion was generated by 3-9-19 composite pulse [24]. NMR spectra acquisition started approximately 1 h after preparation of the protein solution. Eighty millisecond mixing time TOCSY [25,26] and 200 ms mixing time NOESY [27] (only Sigma lysozyme sample) spectra were recorded with $t_1 = 512$, $t_2 = 2048$ and processed with the use of NMRPIPE program [28]. Zero-filling in t_1 domain to 1024 values and by $\pi/2$ shifted sine-bell in both dimensions were applied prior to Fourier transformation. Spectra analysis, and peaks assignment were performed with XEASY [29] program. Assignment process for both samples based on the chemical shift data values published [11] for lysozyme from Sigma. For the Sigma sample the assignment was followed and verified by the detailed analysis of the sequential cross-peaks in the NOESY spectra. Assignment of Trp111 Hα resonance differs from the published data (4.07 ppm instead of 3.72). The assignments of amide and Hα resonances of both lysozyme samples have been deposited at the BioMagResBank database (http://www.bmrb.wisc.edu, access number 4943).

Structural discussion is based on the 1LKS PDB entry of hen-egg white lysozyme [30]. Lattice coordination system was generated using program MICELL written by Wolf [31].

Time-resolved DLS experiments were performed to follow the initial nucleation stages of both lysozyme samples. The experiments were conducted using stock lysozyme concentrations of 1.4, 4.2 and 7.0 mM in Na–acetate buffer, pH 4.25. For inducing aggregation, lysozyme was mixed in an 1:1 ratio with 1.5 M NaCl (dissolved in the same buffer), to attain the final mixture concentration.

The experimental set-up employed for the DLS measurements has been recently built in our laboratory. The apparatus employs a single mode fiber receiving the scattered light at angles between 25 and 155°. The apparatus can accommodate disposable round glass cells with 5 mm diameter and DLS measurements can be performed in 50 μl of solution. A 100 mW frequency doubled laser operating at 532 nm serves as light source. The signals are directed to an ALV SO-SIPD photon detector and after amplification and discrimination to an ALV-5000E digital correlator. Data evaluation of the spectra is performed using a Laplace inversion technique (Provencher) [32,33]. All experiments were conducted at a scattering angle of 32° and at 293.2 K (in an air-conditioned room).

Both lysozyme types were crystallized under the same conditions employed in the DLS experiments using standard 6 μl hanging drop technique. Crystal growth was followed daily with observations under a stereo microscope.

Acknowledgments

This work was supported by a Deutsche Forshungsgemeinschaft (Sa 196/126-2) grant to Y.G. and by an EC grant (B104-CT98-0086) to L.W. and we thank Dr A.M. Kierzek and Dr A. Wyslouch for discussions and Mrs H. Evers for expert technical assistance. The authors are indebted to the Laboratory of Biological NMR (IBB PAS) for the access to the NMR spectrometer and to the Laboratory of the Biological Mass Spectrometry (IBB PAS) for the access to the MS spectrometer. Thanks also belong to the Greek Secretary of Research and Technology for financial support to TRITON-HELLAS through the Greek-Polish cooperation program (EPAN-M.4.3 [2013555]).

References

[1] Y. Georgalis, W. Saenger, Light scattering studies in nucleating lysozyme solutions, research trends, Curr. Top. Crystal Growth Res. 4 (1998) 1–62.

[2] M. Muschol, F. Rosenberger, Interactions in undersaturated and supersaturated lysozyme solutions: static and dynamic light scattering results, J. Chem. Phys. 103 (1995) 10424–10432.

[3] M. Muschol, F. Rosenberger, Lack of evidence for prenucleation aggregate formation in lysozyme crystal growth solutions, J. Crystal Growth 167 (1996) 738–747.

[4] R.F. Xiao, D.J.I. Alexander, F. Rosenberger, The morphological evolution of a growing crystal, Phys. Rev. A 38 (1988) 2447–2456.

[5] D.J.I. Alexander, Lattice models, in: J.P. van der Eerden, O.S.L. Bruinsma (Eds.), Science and Technology of Crystal Growth, Kluwer Academic Publishers, The Netherlands, 1995, pp. 81–95.

[6] S. Tanaka, M. Yamamoto, K. Kawashima, K. Ito, R. Hayagawa, M. Ataka, Kinetic study on the early stage of the crystallization process of two forms of lysozyme crystals by photon correlation spectroscopy, J. Crystal Growth 168 (1996) 44–49.

[7] J.S. Langer, An introduction to the kinetics of first-order phase transition, in: C. Godreché (Ed.), Solids Far from Equilibrium, Cambridge University Press, Cambridge, 1992, pp. 297–361.

[8] S. Tanaka, M. Yamamoto, K. Ito, R. Hayagawa, M. Ataka, Relation between the phase separation and the crystallization in protein solutions, Phys. Rev. E 56 (1997) R67–R69.

[9] B.J. Berne, R. Pecora, Dynamic Light Scattering: With Applications to Chemistry, Biology, and Physics, Dover Publications, Dover, 2000.

[10] W. Brown, Dynamic Light Scattering, The Method and some Applications, Oxford Science Publications, London, 1993.

[11] C. Redfield, C.M. Dobson, Sequential ^{1}H NMR assignments and secondary structure of hen egg white lysozyme in solution, Biochemistry 27 (1988) 122–136.

[12] P.R. Wills, Y. Georgalis, Concentration dependence of the diffusion coefficient of a dimerizing protein: bovine pancreatic trypsin inhibitor, J. Phys. Chem. 85 (1981) 3978–3984.

[13] W. Eberstein, Y. Georgalis, W. Saenger, Molecular interactions in crystallizing lysozyme solutions studied by photon correlation spectroscopy, J. Crystal Growth 143 (1994) 71–78.

[14] Y. Georgalis, P. Umbach, D.M. Soumpasis, W. Saenger, Ordering of fractal nuclei in crystallizing lysozyme solutions, J. Am. Chem. Soc. 121 (1999) 1627–1635.

[15] Y. Georgalis, P. Umbach, J. Raptis, W. Saenger, Lysozyme aggregation studied by light scattering I: influence of concentration and nature of electrolytes, Acta Crystallog. D 53 (1997) 691–702.

[16] Y. Georgalis, P. Umbach, J. Raptis, W. Saenger, Lysozyme aggregation studied by light scattering II: variations of protein concentration, Acta Crystallog. D 53 (1997) 703–712.

[17] D.M. Soumpasis, Y. Georgalis, Potential of mean force treatment of salt mediated protein crystallization, Biophys. J. 72 (1997) 2770–2774.

[18] Y. Georgalis, P. Umbach, D.M. Soumpasis, W. Saenger, Dynamics and microstructure formation during nucleation of lysozyme solutions, J. Am. Chem. Soc. 120 (1998) 5539–5548.

[19] P. Meakin, Fractals, Scaling and Growth Far from Equilibrium, Cambridge University Press, Cambridge, 1998.

[20] M. Buck, J. Boyd, C. Redfield, et al., Structural determinants of protein dynamics: analysis of ^{15}N NMR relaxation measurements for main-chain and side-chain nuclei of hen egg white lysozyme, Biochemistry 34 (1995) 4041–4055.

[21] T. Haliloglu, I. Bahar, Structure-based analysis of protein dynamics: comparison of theoretical results for hen lysozyme with X-ray diffraction and NMR relaxation data, Proteins 37 (1999) 654–667.

[22] D.J. States, R.A. Haberkorn, D.J. Ruben, A two-dimensional nuclear Overhauser experiment with pure absorption phase in four quadrants, J. Magn. Res. 48 (1982) 286–292.

[23] M. Piotto, V. Saudek, V. Sklenar, Gradient-tailored excitation for single-quantum NMR spectroscopy of aqueous solutions, J. Biomol. NMR 2 (1992) 661–665.

[24] V. Sklenar, M. Piotto, R. Lepik, V. Saudek, Gradient-tailored water suppression for ^{1}H–^{15}N HSQC experiments optimized to retain full sensitivity, J. Magn. Res. 102 (1992) 241–245.

[25] D.G. Davis, A. Bax, Assignment of complex ^{1}H NMR spectra via two-dimensional homonuclear Hartmann–Hahn spectroscopy, J. Am. Chem. Soc. 107 (1985) 2820–2821.

[26] C. Griesinger, G. Otting, K. Wüthrich, R.R. Ernst, Clean TOCSY for ^{1}H spin system identification in macromolecules, J. Am. Chem. Soc. 110 (1988) 7870–7872.

[27] J. Jeener, B.H. Meier, P. Bachmann, R.R. Ernst, Investigation of exchange processes by two-dimensional NMR spectroscopy, J. Chem. Phys. 71 (1979) 4546–4553.

[28] F. Delaglio, S. Grzesiek, G.V. Vuister, G. Zhu, J. Pfeifer, A. Bax, NMRPIPE: a multidimensional spectral processing system based on UNIX pipes, J. Biomol. NMR 6 (1995) 277–293.

[29] C. Bartels, T.E. Xia, M. Billeter, P. Guntert, K. Wüthrich, The Program XEASY for the computer-supported NMR spectral analysis of biological macromolecules, J. Biomol. NMR 5 (1995) 1–10.

[30] L.K. Steinrauf, Structures of monoclinic lysozyme iodide at 1.6 Å and of triclinic lysozyme nitrate at 1.1 Å, Acta Crystallog. D 54 (1998) 767–780.

[31] A.M. Kierzek, W.M. Wolf, P. Zielenkiewicz, Simulations of nucleation and early growth stages of protein crystals, Biophys J. 73 (1997) 571–580.
[32] S.W. Provencher, A constrained regularization method for inverting data represented by noisy linear algebraic or integral equations, Comp. Phys. Comm. 27 (1982) 213–227.
[33] S.W. Provencher, A constrained regularization method for inverting noisy linear algebraic or integral equations, Comp. Phys. Comm. 27 (1982) 229–242.